Multi-modal wave propagation in smart structures with shunted piezoelectric patches

T.L.Huang · M.N.Ichchou · O.A.Bareille · M.Collet · M.Ouisse

Abstract The propagation of wave modes in elastic structures with shunted piezoelectric patches is dealt with in this work. The Wave Finite Element(WFE) approach, which is based on the finite element(FE) method and periodical structure theory, is firstly developed as a prediction tool for wave propagation characteristics in beam like structures, and subsequently extended to consider shunted piezoelectric elements through the Diffusion Matrix Model(DMM). With these numerical techniques, reflection and transmission coefficients of propagating waves in structures with shunted piezoelectric patches can be calculated. The performance of shunted piezoelectric patches on the control of wave propagation is investigated numerically with the DMM. Forced response of the smart structure can also be calculated, and based on which the time response of the structure can be obtained via an Inverse Discrete Fourier Transform(IDFT) approach. These general formulations can be applied to all types of slender structures. All these numerical tools can facilitate design modifications and systematic investigations of geometric and electric parameters of smart structures with shunted piezoelectric elements.

T.L.Huang, M.N.Ichchou*, O.A.Bareille

LTDS UMR5513 Ecole Centrale de Lyon, 36 Avenue Guy de Collongue, 69130 Ecully, France

*Corresponding author. E-mail: mohamed.ichchou@ec-lyon.fr. Tel.: +(33)4 72 18 62 30. Fax: +(33)4 72 18 91 44

M.Collet, M.Ouisse

FEMTO-ST, Department of Applied Mechanics, UMR-CNRS 6174, 24 Chemin de l'Epitaphe, 25000 Besançon, France

1 Introduction

Recently, a revolution has taken place in the field of integrated micro-electromechanical systems(MEMS) that offers new opportunities for smart structure design and optimization. The next generation of smart composite structures [1,2] is able to be created via the mechanical integration of active smart materials, electronics, chip sets and power supply systems. The material's intrinsic passive mechanical behavior can be controlled through electromechanical transducers in order to attain new desired functionalities [3]. Among the control configurations found in published works, a well-known technique is the piezoelectric damping using external resistor-inductor shunt circuit [3–9]. This semi-active configuration has the advantage of guaranteeing stability, and can be obtained by bonding piezoelectric elements onto a structure and connecting the electrodes to the external shunt circuit. Due to straining of the host structure, and through the direct piezoelectric effect, a portion of the mechanical energy is converted into electrical energy and subsequently be dissipated by Joule heating via the connected resistor. The $R - L$ shunt circuit on piezoelectric patches can be regarded as light oscillators instead of heavy mass-spring structures. By varying the inductance L in the shunt circuit, the tuning frequency can be adjusted to desired fre-

quency band.

In order to analyze and design structures with piezoelectric elements, techniques for the prediction of dynamical behavior of this kind of structure have been developed. At first, analytical models have been proposed. A uniform strain model for a beam with piezoelectric actuators bonded on the surface or embedded in it was developed in the work of Crawley and de Luis [10]. This model also incorporated shear lag effects of the adhesive layer the piezoelectric actuator and the beam. In the work of Lee [11], induced strain was treated as equivalent thermal effects, and a model based on classical laminate theory was presented. Zhang and Sun [12] constructed a new adaptive sandwich structure using the shear mode of piezoelectric materials. Governing equations for the proposed beam and its surface-mounted counterpart are derived based on the variational principle. And later, Hu and Yao [13] derived the elasticity solution of PZT generated wave propagation in terms of the wave reflection and transmission matrices based on the Timoshenko beam theory. Hagood and von Flotow [4] provided a comprehensive description of the dynamic of shunted piezoelectric patch. Based on the work of Hagood and von Flotow [4], Park [14] studied the vibration attenuation of beams via shunted piezoelectric elements, and proposed a mathematical model to describe the flexural vibration behavior of a cantilevered

beam system with resonant shunt circuits.

The development of the finite element method(FEM) enabled the numerical modeling of various structures with piezoelectric elements [15]. It is an effective tool for the prediction of structural dynamic behavior as it possesses the advantages of widespread use in the engineering domain and the capability of treating complex geometry. Structures with shunted piezoelectric elements were treated properly with FEM [7,8]. However, the excessive computational time associated with large models constitutes one of the major limitations of this method. As an alternative, the numerical description of waves traveling into waveguides and slender structures like beams can be applied. This description provides a low cost and efficient way to capture the dynamic behavior of those structures as it only requires the treatment of a typical unit subsystem [16] whose sizes are related to the cross-section dynamics only. The Wave Finite Element(WFE) method [17–19], which is based on the classic finite element description of a typical cell extracted from a given global system, is an appropriate tool for the prediction of wave propagation in waveguides such as beams [20,21] and plates [22,23] in a wide frequency band. It is also known that the transfer matrix method can be applied to calculate the wave propagation in periodic or nearly periodic structures [24, 25]. However, this method is less advantageous than the

WFE and DMM approaches, as the latter give full finite element description of the waveguide's cross-section dynamics, for the coupling element as well. Model reduction techniques can also be applied in the WFE and DMM approaches.

Recently, Spadoni *et al.* [6] and Casadei *et al.* [9] have studied the control of wave propagation in plates with periodic arrays of shunted piezoelectric patches. Efforts have been dedicated firstly to developing the finite element formulation of shunted piezoelectric elements, then to characterizing the dispersion relation of waves propagating over the surface of plate structures and the band gaps in the frequency domain. An experimental investigation was carried out in the work of Casadei *et al.* [9] to test the performance of shunted piezoelectric patches via the forced response of the structure. Wang *et al.* [26] has realized the same analysis on a beam with periodic shunted piezoelectric patches through an analytical model and corresponding experimental tests. Collet *et al.* [3] provided a full finite element description of a beam with periodic shunted piezoelectric patches via the WFE method, but emphasis was placed on the optimization of shunt impedance. The energy diffusion is supposed to occur at the interface between the part of the beam without shunted piezoelectric patches and the part of the beam with a set of periodic shunted piezoelectric patches. The energy diffusion

related to a unit cell in the set of periodic patches is not analyzed. Suitable numerical tools which can characterize energy diffusion properties for structures with shunted piezoelectric elements still need to be properly developed. These tools will be applied for intensive computations aiming at the design of the piezoelectric patch and the electronic shunt circuit on the patch.

In this work, general formulations for smart structures with shunted piezoelectric patches are proposed. These formulations can be applied for all kinds of slender smart structures. On the whole, this paper focuses on two main objectives:

1. Offering efficient numerical tools for the prediction of wave propagation characteristics and dynamic behavior such as reflection and transmission coefficients of the wave modes, frequency and time responses of beam structures with a pair of shunted piezoelectric patches so as to design properly this kind of smart structures. Optimization of the unit cell in the periodic set of piezoelectric patches can be carried out with these tools to obtain optimal geometric and electric parameters.

2. Providing effective verification and validation approaches to evaluate wave propagation characteristics and dynamic behavior in order to test the efficiency of all the numerical techniques.

This article is organized as follows: in Section 2, a brief outline of the WFE approach is provided (Subsection 2.1). Then the numerical tool to predict the energy diffusion of the flexural wave mode in the beam with shunted piezoelectric patches is presented (Subsection 2.2). Thereafter, the numerical tool to evaluate the forced response of the structure, namely the Forced Wave Finite Element(FWFE) approach, is described (Subsection 2.3). The approach to acquire time response of the structure is introduced in Subsection 2.4. All these numerical techniques are applied in Section 3, where 3 study cases are investigated carefully. Besides the performance of the shunted piezoelectric patches on the control of flexural wave mode in the beam, the influence of the orientation (longitudinal or transversal) of these patches is tested as well. Subsequently, the beam is excited in the tension/compression mode with a wave packet excitation, and corresponding frequency and time responses are calculated, based on which the reflection coefficients can be extracted to verify DMM simulation results. Concluding remarks and perspectives of this work are presented in Section 4.

2 Outline of the numerical prediction tools for smart structures with shunted piezoelectric elements

In this section, firstly the WFE formulation and the DMM are presented. Then the numerical models of beams with shunted piezoelectric elements are described in detail. The finite element diffusion model proposed in the work of Mencik and Ichchou [17] was extended to consider piezoelectric elements. All these techniques enable the calculation of parameters like reflection and transmission coefficients, the frequency response function, and the time response of the structure under wave packet excitation, so as to investigate the influence of the shunted piezoelectric patches on the propagation of wave modes in the beam. The formulations developed are general and can be employed for all types of slender structures with shunted piezoelectric patches.

2.1 Wave propagation and diffusion in structures through finite elements

The WFE method was employed to study the energy diffusion problem [17,27,28]. These references provide a detailed description of the dynamical behavior of a slender structure, as illustrated in Figure 1, which is composed, along a specific direction (say $X-$axis), of N identical substructures. Note that this general de-

scription can be applied to homogeneous systems whose cross-sections are constant. The dynamic of the global system is formulated from the description of the waves propagating along the $X-$axis.

Figure 1

Let us consider a finite element model of a given substructure k ($k \in \{1, \ldots, N\}$) belonging to the waveguide (cf. Figure 1). The left and right boundaries of the discretized substructure are assumed to contain n degrees of freedom (DOFs). Displacements $\mathbf{q}$ and forces $\mathbf{F}$ which are applied on these boundaries are denoted by $(\mathbf{q}_{\mathrm{L}}, \mathbf{q}_{\mathrm{R}})$ and $(\mathbf{F}_{\mathrm{L}}, \mathbf{F}_{\mathrm{R}})$, respectively. It is assumed that the kinematic quantities are represented through state vectors $\mathbf{u}_{\mathrm{L}}^{(k)} = ((\mathbf{q}_{\mathrm{L}}^{(k)})^{\mathrm{T}}(-\mathbf{F}_{\mathrm{L}}^{(k)})^{\mathrm{T}})^{\mathrm{T}}$ and $\mathbf{u}_{\mathrm{R}}^{(k)} = ((\mathbf{q}_{\mathrm{R}}^{(k)})^{\mathrm{T}}(\mathbf{F}_{\mathrm{R}}^{(k)})^{\mathrm{T}})^{\mathrm{T}}$, and that the internal DOFs of substructure k are not submitted to external forces. According to Mencik and Ichchou [17], the continuity conditions between the substructures combined with the periodicity condition and the dynamical equilibrium of each substructure can finally lead to the following boundary value problem:

$$\mathbf{S}\boldsymbol{\Phi}_i = \mu_i \boldsymbol{\Phi}_i \quad , \quad |\mathbf{S} - \mu_i \mathbf{I}_{2n}| = \mathbf{0}. \tag{1}$$

According to [3], the eigenvalues μ_i and wavenumbers k_i are linked through the relation $\mu_i = e^{-ik_i d_x}$, where d_x denotes the length of the unit cell in X-axis. The real part of the wavenumber $k_i, Re(k_i)$, represents the direction of the phase velocity of the corresponding waves:

if $Re(k_i) > 0$, the phase propagates in the positive x direction; if $Re(k_i) < 0$, the phase propagates in the negative direction, and if it is zero, k_i corresponds to the wavenumber of a pure evanescent wave that only occurs when an undamped system is considered [23]. The matrix $\mathbf{\Phi}$ of the eigenvectors can be described in this way:

$$\mathbf{\Phi} = \begin{bmatrix} \mathbf{\Phi}_{\mathbf{q}}^{\mathtt{inc}} & \mathbf{\Phi}_{\mathbf{q}}^{\mathtt{ref}} \\ \mathbf{\Phi}_{\mathbf{F}}^{\mathtt{inc}} & \mathbf{\Phi}_{\mathbf{F}}^{\mathtt{ref}} \end{bmatrix}, \tag{2}$$

where subscripts $\mathbf{q}$ and $\mathbf{F}$ refer to the components which are related to the displacements and the forces, respectively; $((\mathbf{\Phi}_{\mathbf{q}}^{\mathtt{inc}})^{\mathtt{T}}(\mathbf{\Phi}_{\mathbf{F}}^{\mathtt{inc}})^{\mathtt{T}})^{\mathtt{T}}$ and $((\mathbf{\Phi}_{\mathbf{q}}^{\mathtt{ref}})^{\mathtt{T}}(\mathbf{\Phi}_{\mathbf{F}}^{\mathtt{ref}})^{\mathtt{T}})^{\mathtt{T}}$ stand for the modes which are incident to and reflected by a specific boundary (left or right) of the heterogeneous waveguide, respectively. Finally, assuming modal decomposition, state vectors $\mathbf{u}_{\mathtt{L}}^{(k)}$ and $\mathbf{u}_{\mathtt{R}}^{(k)}$ of any substructures k can be expressed from eigenvectors $\{\mathbf{\Phi}_i\}_{i=1,\ldots,2n}$ [16]:

$$\mathbf{u}_{\mathtt{L}}^{(k)} = \mathbf{\Phi}\mathbf{Q}^{(k)} \quad , \quad \mathbf{u}_{\mathtt{R}}^{(k)} = \mathbf{\Phi}\mathbf{Q}^{(k+1)} \quad \forall k \in \{1,\ldots,N\}. \tag{3}$$

Here, vector $\mathbf{Q}$ stands for the amplitudes of the wave modes, which can be expressed by (cf.Equation (2)):

$$\mathbf{Q} = \begin{pmatrix} \mathbf{Q}^{\mathtt{inc}} \\ \mathbf{Q}^{\mathtt{ref}} \end{pmatrix}. \tag{4}$$

The dynamical behavior of a periodic waveguide can be simply expressed from a basis of modes representing waves traveling in the positive and negative directions of the system. An analysis of the dynamical response consists of evaluating a set of amplitudes $\{(\mathbf{Q}^{\mathtt{inc}(k)}, \mathbf{Q}^{\mathtt{ref}(k)})\}_k$ associated with the incident and reflected modes. Nevertheless, to evaluate energy diffusion, the formulation of the boundary conditions of the system is needed, and particularly at a coupling junction where several waveguides can be considered. It should be mentioned that the whole system has free boundary conditions, and the coupling conditions are in fact boundary conditions for subsystems(waveguides and coupling element).

In order to characterize, in terms of wave modes, the coupling conditions between two different periodic waveguides, the two systems are assumed to be connected, in a general manner, via an elastic coupling element (see Figure 2). This study aims to predict the dynamics of complex systems which are composed of two periodic waveguides.

Figure 2

Let us consider two periodic waveguides which are coupled through a coupling element and let us consider two corresponding substructures (1 and 2) which are located at the ends of the waveguides (see Figure 2). These substructures are coupled with the coupling element at surfaces Γ_1 and Γ_2 and are coupled with the other substructures, into waveguides, at surfaces S_1 and S_2. It is assumed that the coupling element is only sub-

ject to the coupling actions (i.e. there is no force inside the element).

According to Mencik and Ichchou [17], with the dynamical equilibrium of the wave guides and the coupling element, and their continuity conditions of nodal displacement and force expressed in the modal basis, it can be demonstrated that the dynamical behavior of a given coupled periodic waveguide i $(i = 1, 2)$ can be simply expressed in terms of wave modes incident to the coupling element $((\mathbf{\Phi_q^{inc(i)}})^T(\mathbf{\Phi_F^{inc(i)}})^T)^T$, and wave modes reflected by the coupling element $((\mathbf{\Phi_q^{ref(i)}})^T(\mathbf{\Phi_F^{ref(i)}})^T)^T$. In this sense, it can be proved that amplitudes $(\mathbf{Q^{ref(1)}}, \mathbf{Q^{ref(2)}})$ of the modes reflected by the coupling element can be related to amplitudes $(\mathbf{Q^{inc(1)}}, \mathbf{Q^{inc(2)}})$ of the modes incident to the coupling element via a diffusion matrix, namely $\mathbb{C}$, which relates the reflection and transmission coefficients of the wave modes through the dynamical behavior of the coupling element:

$$\begin{pmatrix} \mathbf{Q^{ref(1)}} \\ \mathbf{Q^{ref(2)}} \end{pmatrix} = \mathbb{C} \begin{pmatrix} \mathbf{Q^{inc(1)}} \\ \mathbf{Q^{inc(2)}} \end{pmatrix}, \tag{5}$$

The diffusion matrix $\mathbb{C}$ directly depends on the normalization of eigenvectors $\{\mathbf{\Phi}_j^{(1)}\}_j$ and $\{\mathbf{\Phi}_k^{(2)}\}_k$. It seems advantageous to normalize the eigenvectors of the two waveguides in a similar manner.

2.2 Piezoelectric finite element formulation for the coupling element

In the Diffusion Matrix Model(DMM) [27], in order to consider properly a coupling element with shunted piezoelectric patches, an appropriate formulation should be used. Firstly, the three-dimensional piezoelectric constitutive law can be written as:

$$T = \mathbf{c}^E S - \mathbf{e^T} E \tag{6a}$$

$$D = \mathbf{e} S + \epsilon^S E \tag{6b}$$

where E denotes the electric field vector, T the mechanical stress vector, S the mechanical strain, and D the electric displacement vector; $\mathbf{c}^E$ represents the material stiffness matrix, $\mathbf{e}$ denotes the piezoelectric stress coupling matrix, and ϵ^S is the permittivity matrix under constant strain. Equation (6a) represents the indirect piezoelectric effect, whereas Equation (6b) characterizes the direct piezoelectric effect. A finite element model of the coupled system consisting of a beam and a pair of identic piezoelectric patches with shunted circuit is then established, as displayed in Figure 3.

Figure 3

This model contains two waveguides with 3D linear brick finite elements and a coupling element with 3D linear brick piezoelectric finite elements. The piezoelectric element has 8 nodes and 4 degrees of freedom(DOF)

per node. Each node has 3 structural DOF and 1 electrical DOF (electrical potential). All electrical potential DOF that are placed on electrode surfaces of the patches are reduced such that only one potential master DOF remains. All electrical potential DOF on the patch surfaces bonded to the beam are grounded. The whole structure has free mechanical boundary conditions. For the sake of simplicity, detailed deductions of strain energy, mass and stiffness matrices for the piezoelectric elements (without shunt circuit), which can be found in the work of Casadei $et\ al.$ [9], are not presented in this paper. The discretized electro-elastic system of equations can be written in the form shown in Equation (7a) and Equation (7b).

$$\mathbf{M}_{dd}\ddot{d} + \mathbf{K}_{dd}d + \mathbf{K}_{dv}V = \mathbf{f} \tag{7a}$$

$$\mathbf{K}_{dv}^{\mathbf{T}}d + \mathbf{K}_{vv}V = \mathcal{Q} \tag{7b}$$

where d and V represent the structural and electrical DOF respectively, and:

$$\mathbf{M}_{dd} = \int_{V_s} \mathbf{N}_d^{\mathbf{T}}\rho\mathbf{N}_d dV, \quad \mathbf{K}_{dd} = \int_{V_s} \mathbf{B}_d^{\mathbf{T}}\mathbf{c}^E\mathbf{B}_d dV, \quad \mathbf{K}_{dv} = \int_{V_s} \mathbf{B}_d^{\mathbf{T}}\mathbf{e}^{\mathbf{T}}\mathbf{B}_v dV$$

$$\mathbf{K}_{vv} = \int_{V_s} \mathbf{B}_v^{\mathbf{T}}\epsilon^s\mathbf{B}_v dV, \quad \mathbf{f} = \int_{S_f} \mathbf{N}_d^{\mathbf{T}}f dS, \quad \mathcal{Q} = \int_{S_q} \mathbf{N}_v^{\mathbf{T}}q dS. \tag{8}$$

in which $\mathbf{N}_d$ and $\mathbf{N}_v$ are the shape functions, $\mathbf{B}_d = \mathcal{D}\mathbf{N}_d$ and $\mathbf{B}_v = \nabla\mathbf{N}_v$. $\mathcal{D}$ is the linear differential operator matrix which relates the strains to the structural displacements U. In this case, the matrix $\mathcal{D}$ is given in Equation (9).

$$\mathcal{D} = \begin{pmatrix} \frac{\partial}{\partial x} & 0 & 0 \\ 0 & \frac{\partial}{\partial y} & 0 \\ 0 & 0 & \frac{\partial}{\partial z} \\ \frac{\partial}{\partial y} & \frac{\partial}{\partial x} & 0 \\ 0 & \frac{\partial}{\partial z} & \frac{\partial}{\partial y} \\ \frac{\partial}{\partial z} & 0 & \frac{\partial}{\partial x} \end{pmatrix} \tag{9}$$

After finite element assembly, the discretized coupled piezoelectric and structural field equations are finally given in terms of nodal displacements u and nodal electric potential φ. Following the electrode definitions mentioned in the work of Becker $et\ al.$ [8], the electrical potential DOF in the piezoelectric patches are partitioned into three different groups:

– For nodes on the outer surfaces of the piezoelectric patches, their associated electrical DOF are called φ_p, and they have the same electrical potential;

– For nodes on the inner surfaces of the piezoelectric patches bonded to the beam, their associated electrical DOF are called φ_g, and they are grounded;

– For nodes inside the piezoelectric patches, their associated electrical DOF are called φ_i.

The equations of motion are subsequently written in the form shown in Equation (10).

$$\begin{bmatrix} \mathbf{M}_{uu} & 0 & 0 & 0 \\ 0 & 0 & 0 & 0 \\ 0 & 0 & 0 & 0 \\ 0 & 0 & 0 & 0 \end{bmatrix}\begin{bmatrix} \ddot{u} \\ \ddot{\varphi}_i \\ \ddot{\varphi}_p \\ \ddot{\varphi}_g \end{bmatrix} + \begin{bmatrix} \mathbf{K}_{uu} & \mathbf{K}_{ui} & \mathbf{K}_{up} & \mathbf{K}_{ug} \\ \mathbf{K}_{ui}^{\mathbf{T}} & \mathbf{K}_{ii} & \mathbf{K}_{ip} & \mathbf{K}_{ig} \\ \mathbf{K}_{up}^{\mathbf{T}} & \mathbf{K}_{ip}^{\mathbf{T}} & \mathbf{K}_{pp} & \mathbf{K}_{pg} \\ \mathbf{K}_{ug}^{\mathbf{T}} & \mathbf{K}_{ig}^{\mathbf{T}} & \mathbf{K}_{pg}^{\mathbf{T}} & \mathbf{K}_{gg} \end{bmatrix}\begin{bmatrix} u \\ \varphi_i \\ \varphi_p \\ \varphi_g \end{bmatrix} = \begin{bmatrix} \mathbf{F} \\ \mathcal{Q}_i \\ \mathcal{Q}_p \\ \mathcal{Q}_g \end{bmatrix} \tag{10}$$

As $\varphi_g = 0$, the fourth equation and fourth column in the mass and stiffness matrices can be eliminated. Internal potential DOF can be determined by exact static condensation from Equation (10) since internal electric charges $\mathcal{Q}_i = 0$:

$$\varphi_i = -\mathbf{K}_{ii}^{-1}\mathbf{K}_{ui}^{\mathbf{T}}u - \mathbf{K}_{ii}^{-1}\mathbf{K}_{ip}\varphi_p \tag{11}$$

Since all the nodes on the potential electrode surfaces have identical potentials, an explicit transformation matrix $\mathbf{T_m}$ can be used to define the master potential DOF φ_m, as shown in Equation (12).

$$\varphi_p = \mathbf{T_m}\varphi_m \tag{12}$$

The use of Equation (12) yields the fully coupled dynamics:

$$\begin{bmatrix} \mathbf{M}_{uu} & 0 \\ 0 & 0 \end{bmatrix} \begin{bmatrix} \ddot{u} \\ \ddot{\varphi}_m \end{bmatrix} + \begin{bmatrix} \mathbf{H}_{uu} & \mathbf{H}_{up} \\ \mathbf{H}_{up}^{\mathbf{T}} & \mathbf{H}_{pp} \end{bmatrix} \begin{bmatrix} u \\ \varphi_m \end{bmatrix} = \begin{bmatrix} \mathbf{F} \\ \mathcal{Q}_m \end{bmatrix} \tag{13}$$

with

$$\mathbf{H}_{uu} = \mathbf{K}_{uu} - \mathbf{K}_{ui}\mathbf{K}_{ii}^{-1}\mathbf{K}_{ui}^{\mathbf{T}} \tag{14a}$$

$$\mathbf{H}_{up} = (\mathbf{K}_{up} - \mathbf{K}_{ui}\mathbf{K}_{ii}^{-1}\mathbf{K}_{ip})\mathbf{T}_m \tag{14b}$$

$$\mathbf{H}_{pp} = \mathbf{T}_m^{\mathbf{T}}(\mathbf{K}_{pp} - \mathbf{K}_{ip}^{\mathbf{T}}\mathbf{K}_{ii}^{-1}\mathbf{K}_{ip})\mathbf{T}_m \tag{14c}$$

$$\mathcal{Q}_m = \mathbf{T}_m^{\mathbf{T}}\mathcal{Q}_p \tag{14d}$$

After the definition of the master DOF, the R-L shunt circuit can be considered. The electrical impedance of the circuit under harmonic excitation can be written as:

$$Z_{sh} = R + j\omega L \tag{15}$$

The current I_{sh} in the shunt circuit can be expressed as Equation (16)

$$I_{sh} = j\omega \mathcal{Q}_m = \frac{\varphi_m}{Z_{sh}} \tag{16}$$

By substituting Equation (16) into Equation (13), the electrical DOF can be condensed and the equation that governs the structural dynamics under harmonic excitation is shown in Equation (17).

$$[\mathbf{H}_{uu} - \omega^2\mathbf{M}_{uu} + \mathbf{H}_{up}(\frac{1}{j\omega Z_{sh}} - \mathbf{H}_{pp})^{-1}\mathbf{H}_{up}^{\mathbf{T}}]u = \mathbb{D}u = \mathbf{F} \tag{17}$$

Equation (17) gives a full finite element description of the beam with two symmetric shunted piezoelectric patches as a coupling element for the DMM calculation. Matrix $\mathbb{D}$ represents the dynamical stiffness matrix of the coupling element.

2.3 Forced Wave Finite Element formulation

The WFE formulation provides wave propagation predictions under free boundary conditions. In order to obtain the forced response of the structure, the Forced Wave Finite Element(FWFE) formulation [18, 29, 30] can be employed. As mentioned in section 2.1, based on Equation (3) and Equation (4), amplitudes $\mathbf{Q}^{(k)}$ which reflect

for instance the kinematic variable $\mathbf{u}_L^{(k)}$ for substructure k, are described from amplitudes $\mathbf{Q}^{(1)}$ and $\mathbf{Q}^{(N+1)}$ representing kinematic variables $\mathbf{u}_L^{(1)}$ and $\mathbf{u}_R^{(N)}$ at the waveguide boundaries. According to the coupling relations between two consecutive substructures k and $k-1$ $(k \in \{2, \ldots, N\})$, $\mathbf{q}_L^{(k)} = \mathbf{q}_R^{(k-1)}$ and $-\mathbf{F}_L^{(k)} = \mathbf{F}_R^{(k-1)}$, the following relation can be found:

$$\mathbf{u}_L^{(k)} = \mathbf{u}_R^{(k-1)} \quad \forall k \in \{2, \ldots, N\} \tag{18}$$

which leads to

$$\mathbf{u}_L^{(k)} = \mathbf{S}\mathbf{u}_L^{(k-1)} \quad \forall k \in \{2, \ldots, N\} \tag{19}$$

Equation (19) allows to write:

$$\mathbf{u}_L^{(k)} = \mathbf{S}^{k-1}\mathbf{u}_L^{(1)} \quad \forall k \in \{1, \ldots, N\} \tag{20}$$

with $\mathbf{S}^0 = \mathbf{I}_{2n}$, and:

$$\mathbf{u}_R^{(N)} = \mathbf{S}^N\mathbf{u}_L^{(1)} \tag{21}$$

Equation (20) and Equation (21) are projected on the basis $\{\mathbf{\Phi}_i\}_i$ considering Equation (3). Since matrix $\mathbf{\Phi}$ is invertible (it has been assumed that $det[\mathbf{\Phi}] \neq 0$), one obtains [31]:

$$\mathbf{Q}^{(k)} = \mathbf{\Phi}^{-1}\mathbf{S}^{k-1}\mathbf{\Phi}\mathbf{Q}^{(1)} \quad \forall k \in \{1, \ldots, N+1\} \tag{22}$$

that is (cf. Equation (1))

$$\mathbf{Q}^{(k)} = \begin{bmatrix} \mathbf{\Lambda} & \mathbf{0} \\ \mathbf{0} & \mathbf{\Lambda^{-1}} \end{bmatrix}^{k-1} \mathbf{Q}^{(1)} \quad \forall k \in \{1, \ldots, N+1\} \tag{23}$$

where $\mathbf{\Lambda}$ stands for the $(n \times n)$ diagonal eigenvalue matrix for wave modes propagating in x positive direction, expressed by Equation (24) [31].

$$\mathbf{\Lambda} = \begin{bmatrix} \mu_1 & 0 & \ldots & 0 \\ 0 & \mu_2 & \ldots & 0 \\ \vdots & \vdots & \ddots & \vdots \\ 0 & 0 & \ldots & \mu_n \end{bmatrix} \tag{24}$$

Expressing the boundary conditions of the waveguides in terms of amplitudes $\mathbf{Q}^{(1)}$ and $\mathbf{Q}^{(\mathbb{N}+1)}$ allows us to express, from Equation (23), the dynamics of a given substructure k. In a general manner, the boundary conditions at a specific boundary of the waveguide can be formulated in this way:

$$\mathbf{Q}^{\texttt{ref}} \mid_{\texttt{lim}} = \mathbb{C}\mathbf{Q}^{\texttt{inc}} \mid_{\texttt{lim}} + \mathcal{F} \tag{25}$$

where $\mathbb{C}$ stands for the diffusion matrix of the coupling element, and $\mathcal{F}$ denotes the effects of the excitations sources [18,32]. It is demonstrated in the work of Mencik $et\ al.$ [32] that the general relation in Equation (25) can be applied to describe classical Neumann and Dirichlet boundary conditions. These conditions can be expressed as follows:

$$[\mathbf{0} \mid \mathbf{I}]\,\mathbf{u} = \mathbf{F}_0 \qquad (Neumann) \tag{26a}$$

$$[\mathbf{I} \mid \mathbf{0}]\,\mathbf{u} = \mathbf{q}_0 \qquad (Dirichlet) \tag{26b}$$

They can be rewritten in the following manner via the projection of the state vector $\mathbf{u}$ onto the wave mode

basis (see Equation (3)):

$$\mathbf{\Phi}_\mathbf{F}^{\texttt{inc}}\mathbf{Q}^{\texttt{inc}} + \mathbf{\Phi}_\mathbf{F}^{\texttt{ref}}\mathbf{Q}^{\texttt{ref}} = \mathbf{F}_0 \qquad (Neumann) \qquad (27a)$$

$$\mathbf{\Phi}_\mathbf{q}^{\texttt{inc}}\mathbf{Q}^{\texttt{inc}} + \mathbf{\Phi}_\mathbf{q}^{\texttt{ref}}\mathbf{Q}^{\texttt{ref}} = \mathbf{q}_0 \qquad (Dirichlet) \qquad (27b)$$

2.4 Wave Finite Element method in time domain

Based on frequency response of the structure issued from the FWFE method, the time response of the structure can be obtained in a rather simple way. For example, if a structure is subjected to an excitation force $\mathbf{f}_{\texttt{exc}}$ in time domain $[t_k]_{k=1\dots M}$, through a Discrete Fourier Transform(DFT), the spectrum of this excitation force $\hat{\mathbf{f}}_{\texttt{exc}}$ can be expressed in the frequency domain $[\omega_k]_{k=1\dots M}$.

$$\hat{\mathbf{f}}_{\texttt{exc}}(\omega_k) = \sum_{m=1}^{M} \mathbf{f}_{\texttt{exc}}(t_m)e^{-jt_m\omega_k} \qquad (28)$$

This spectrum is then used in the FWFE approach to calculate the nodal displacement response $\hat{\mathbf{u}}(\omega_\mathbf{m})$ frequency by frequency. Subsequently, by applying an Inverse Discrete Fourier Transform(IDFT) to the frequency response, the time response can be acquired.

$$\mathbf{u}(t_k) = \frac{1}{M}\sum_{m=1}^{M}\hat{\mathbf{u}}(\omega_m)e^{-jt_k\omega_m} \qquad (29)$$

It should be noted that M, the number of samples should be large enough to ensure the quality of the frequency and time response.

3 Numerical simulations of beams with shunted piezoelectric patches

In this section, the DMM with shunted piezoelectric elements is firstly employed to calculate the reflection and transmission coefficients of the Z-axis flexural wave and the X-axis tension/compression wave in the beam. A full finite element description that takes the mechanical-electrical coupling into account is given to the smart structure. The influence of the shunted piezoelectric patches on the propagation of these wave modes is carefully investigated, and an analytical model is developed to verify the numerical results. Subsequently, the FWFE approach is applied for the evaluation of the dynamical behavior of the structure in frequency domain. Unlike the DMM approach which gives predictions for the beam structure with free boundary conditions, frequency response functions can be obtained for the beam structure with forced boundary conditions. Waveguides are of finite length in this case. Thereafter, based on the frequency responses, the calculation of time responses of the structure under wave packet excitation is carried out. An extraction procedure is proposed to calculate reflection coefficients of the X-axis tension/compression mode so as to verify the results issued from the DMM approach.

It should be mentioned that the problem of a piezo-

electric patch shunted through a $R - L$ circuit that acts as a vibration absorber or noise controller has been used extensively in the past and its behavior has been examined thoroughly via analytical or numerical models. However, no numerical tools that can predict wave propagation and diffusion in a unit cell belonging to a set of periodically distributed shunted piezoelectric patches are proposed in the literature. The effects of a piezoelectric patch shunted through a $R - L$ circuit as a vibration absorber on the energy diffusion of a specific wave mode propagating in a slender system are never studied in detail. The focus of the present work lies in the wave propagation and energy diffusion problems in such systems, and new efficient numerical tools aiming at achieving these goals are provided and tested in this section.

3.1 DMM approach applied for Z-axis flexural wave

The structures to be studied here are beams with two symmetric bonded $R - L$ shunted piezoelectric patches. In the first case of study (Case A), the widths of the beam and the patches are the same. The finite element model of the coupling element is shown in Figure 4, with the definition of geometric parameters. The parameter L_{beam} represents the length of the beam involved in the coupling element. Numerical values of those geometric parameters are listed in Table 1. The material of the beam is aluminium and considered as isotropic, with Young's modulus $E_{beam} = 70 \ GPa$ and Poisson's ratio $\nu_{beam} = 0.34$, and density $\rho_{beam} = 2700 \ kg/m^3$. The piezoelectric patches are fabricated by Saint Gobain Quartz (type SG P189) and the corresponding material characteristics are listed in Appendix A. This type of piezoelectric patch works mainly in the 3-1 mode, and the two piezoelectric patches should work in phase (both stretched or compressed) for the control of the tension/compression wave, whereas for the flexural mode, they should work in opposite phase (one stretched, the other compressed).

Figure 4

Table 1

At first, the beam is treated as a waveguide and the corresponding dispersion curves of the wave modes propagating in the beam are extracted via the WFE approach, as shown in Figure 5.

Figure 5

Based on this calculation, the mesh resolution is chosen to be $0.005 \times 0.005 \times 0.002 \ m^3$, as the minimum wavelength of the Z-axis flexural wave mode is about 0.1m in the concerned frequency band. The DMM calculation of this wave mode gives the reflection and transmission coefficients as displayed in Figure 6, with $R = 100 \ \Omega$ and $L = 2 \ H$. The tuning frequency f_{tune} of the piezoelec-

tric patches is about 1340 Hz. In fact, around this frequency, the impedance of the structure is greatly modified by the shunted piezoelectric patches so that the wave propagation characteristics change significantly. The tuning frequency can be calculated according to Equation (30):

$$f_{tune} = \frac{1}{2\pi\sqrt{2LC_{p3}^S}} \tag{30}$$

where $C_{p3}^S = (1-k_{31}^2)C_{p3}^T$ is the capacitance of the piezoelectric patch measured at constant strain, and the 2 in front of L is due to the fact that the two piezoelectric patches are connected in parallel. If each piezoelectric patch has an independent shunt circuit, the 2 in front of L will disappear. The subscript 1 represents the X-axis direction while the subscript 3 denotes the Z-axis direction. k_{31} is the electromechanical coupling coefficient. C_{p3}^T is the capacitance of the piezoelectric patch measured at constant stress. It can be calculated in the following manner:

$$C_{p3}^T = \frac{\epsilon^T A_3}{L_3} \tag{31}$$

where A_3 is the area of the surface of the piezoelectric patch perpendicular to Z-axis, $L_3 = h_{patch}$ is the length of the piezoelectric patch in Z-axis direction.

Figure 6

Thereafter, these numerical results are compared to results derived from an analytical beam model. This beam can be divided into 3 propagation mediums, as shown in Figure 7.

Figure 7

It is a combination of 3 analytical models:

– For wave propagation in the beam, the classical Euler-Bernoulli beam model [33] is employed;

– For the part of the beam covered with 2 piezoelectric patches (Medium 2), a homogenization procedure [34] is applied;

– For the piezoelectric patches with shunted circuit, the model in the work of Hagood and von Flotow [4] is used.

This homogenized Euler-Bernoulli beam model with shunted piezoelectric patches offers analytical solutions to the reflection and transmission coefficients of the flexural wave. Assuming that the Young's modulus and density of the shunted piezoelectric patches are E_{patch} and ρ_{patch}. According to Hagood and von Flotow [4], the shunt circuit modifies the material properties of the piezoelectric patch in the following way:

$$s_{patch\ jj}^{sh} = s_{patch\ jj}^E - \bar{Z}_i^{el} \frac{d_{ij}^2}{\epsilon_i^{\mathbf{T}}} \tag{32a}$$

$$E_{patch\ jj}^{sh} = \frac{\mathbf{c}_{patch\ jj}^E}{1 - k_{ij}^2 \bar{Z}_i^{el}} \tag{32b}$$

where $s_{patch\ jj}^{sh}$ represents the shunted piezoelectric compliance in the jth direction and $s_{patch\ jj}^E$ the mechanical compliance in the jth direction, while $E_{patch\ jj}^{sh}$ de-

notes the shunted piezoelectric stiffness in the jth direction, and $\mathbf{c}^E_{patch\ jj}$ the mechanical stiffness in the jth direction. k_{ij} is the electromechanical coupling coefficient defined as shown in Equation (33a), and d_{ij} is the piezoelectric strain coupling coefficient. $\bar{Z}^{el}_i$ denotes the relative electrical impedance defined as shown in Equation (33b). ϵ^T_i is the permittivity under constant strain in the ith direction.

$$k_{ij} = \frac{d_{ij}}{\sqrt{s^E_{jj}\epsilon^T_i}} \tag{33a}$$

$$\bar{Z}^{el}_i = \frac{j\omega C^T_{pi} Z_{shi}}{j\omega C^T_{pi} Z_{shi} + 1} \tag{33b}$$

In the case of this work, there is no shunt circuit in the 1st(X-axis) and 2nd(Y-axis) directions, so $Z_{sh1} = Z_{sh2} = \infty$ and then $\bar{Z}^{el}_1 = \bar{Z}^{el}_2 = 1$. C^T_{pi} is the capacitance between the surfaces of the piezoelectric patch perpendicular to ith direction (at constant stress). For the considered beam to be homogenized, only the loading in the 1st direction (X-axis) is taken into account, thus the Young's modulus of the piezoelectric patch can be calculated as $E_{patch} = E^{sh}_{patch\ 11}$. The effective Young's Modulus E_{eff} of Medium 2 can subsequently be expressed in the form shown in Equation (34).

$$E_{eff} = E_{beam} \frac{12}{h^3_{eff}}(\frac{h^3_1}{6} + 2d^2_1 h_1) + E_{patch} \frac{12}{h^3_{eff}}(\frac{h^3_2}{6} + 2d^2_2 h_2) \tag{34}$$

where

$$h_{eff} = h_{beam} + 2h_{patch}, h_1 = \frac{1}{2}h_{beam}, h_2 = h_{patch}$$

$$d_1 = \frac{1}{4}h_{beam}, d_2 = \frac{1}{2}(h_{beam} + h_{patch}) \tag{35}$$

The effective density ρ_{eff}, area A_{eff} and moment of inertia I_{eff} are shown in Equation (36a), Equation (36b),

and Equation (36c) respectively.

$$\rho_{eff} = \frac{h_{beam}\rho_{beam}}{h_{beam} + 2h_{patch}} + \frac{2h_{patch}\rho_{patch}}{h_{beam} + 2h_{patch}} \tag{36a}$$

$$A_{eff} = b_{beam}(h_{beam} + 2h_{patch}) \tag{36b}$$

$$I_{eff} = \frac{b_{beam}(h_{beam} + 2h_{patch})^3}{12} \tag{36c}$$

Reflection and transmission coefficients of the flexural wave propagating in the beam in case A are calculated analytically and the results are compared to those acquired through the DMM approach, as shown in Figure 8.

Figure 8

The results issued from the DMM approach and those from the homogenized Euler-Bernoulli model correspond well below 2 kHz. However, at higher frequencies, as the homogenization method becomes inaccurate [35, 36], those two approaches give different predictions of reflection and transmission coefficients of the flexural wave. Furthermore, the Euler-Bernoulli analytical model becomes also incorrect at middle and high frequencies, as its plane wave description of the bending mode is not a priori satisfied in this frequency range [17]. Nevertheless, these two different approaches give the same tuning frequency f_{tune}. On the whole, the prediction performance of the DMM approach is well manifested in this case.

3.2 Application of DMM and FWFE for the choice of configuration

3.2.1 Prediction of reflection and transmission coefficients with DMM

Two other numerical simulations are performed for an aluminium beam with two symmetric bonded shunted piezoelectric patches. All the material properties are the same as those used in case A, but the dimensions piezoelectric patch in these two cases (case B and case C) are $0.03 \times 0.01 \times 0.001\ m^3$, and the dimensions of the beam section are $0.03 \times 0.003\ m^2$. These values are defined according to available materials in the laboratory so that the numerical results can be later validated experimentally. Two different configurations are tested: in case B, the two piezoelectric patches are bonded in the longitudinal direction of the beam, as shown in Figure 9(a), whereas in case C, these patches are bonded transversally on the same beam, as displayed in Figure 9(b). Numerical values of the geometric parameters are listed in Table 1, and there definitions can be found in Figure 9(a) and Figure 9(b).

Figure 9

At first, the dispersion curves of the wave modes propagating in the beam in case B and case C are calculated using the WFE approach. The results are shown in Figure 10. The wavelength of the flexural mode in Z-axis is shown in Figure 11. According to the wavelength, the mesh resolution in these two cases is chosen as $0.005 \times 0.005 \times 0.0015\ m^3$ for the beam, and $0.005 \times 0.005 \times 0.001\ m^3$ for the patches. In the frequency band from 0 to 5 kHz, for the Z-axis flexural wave mode, this mesh resolution is fine enough.

Figure 10

Figure 11

The DMM approach is applied subsequently to calculate the reflection and transmission coefficients of the Z-axis flexural wave in the two cases, with $R = 100\ \Omega$ and $L = 2\ H$ in the shunt circuit. The results are shown in Figure 12.

Figure 12

It can be observed from the DMM results that the propagation of the flexural wave is tuned around 1.5 kHz, as the reflection and transmission coefficients vary significantly. The tuning frequency calculated according to Equation (30) is about 1550 Hz, which is quite consistent with the results Figure 12(a) and Figure 12(b). It can also be concluded that the longitudinally bonded shunted piezoelectric patches (case B) results in a higher reflection of the flexural wave mode in the beam than those bonded transversally (case C).

3.2.2 Forced response prediction with FWFE

In order to predict the forced response of the beam with shunted piezoelectric patches, the FWFE method mentioned in Subsection 2.3 can be applied. The same beam with a pair of shunted piezoelectric patches in case B is taken as an example, as displayed in Figure 13(a).

Figure 13

To calculate the forced response, boundary conditions and the lengths of the waveguides should be specified. As shown in Figure 13(a), one extremity of the beam is excited by a punctual force $\mathbf{F}_{\mathtt{exc}}$, and the other extremity is free. The amplitude of the excitation force remains constant in the frequency domain. The first waveguide consists of N_1 identical unit cells while the second one consists of N_2 identical unit cells. The part of the beam covered with the pair of shunted piezoelectric patches is considered to be the coupling element. For the sake of simplicity, it is assumed that $N_1 = N_2 = N$. The two waveguides are identical as they belong to the same beam, thus $\boldsymbol{\Lambda}_1^{\mathtt{inc}} = \boldsymbol{\Lambda}_2^{\mathtt{ref}} = \boldsymbol{\Lambda}$, and $\boldsymbol{\Lambda}_1^{\mathtt{ref}} = \boldsymbol{\Lambda}_2^{\mathtt{inc}} = \boldsymbol{\Lambda}^{-1}$(see Equation (24)). The boundary conditions of the system can be written in the following manner:

$$\boldsymbol{\Phi}_{\mathbf{F1}}^{\mathtt{inc}}\mathbf{Q}_1^{\mathtt{inc}(1)} + \boldsymbol{\Phi}_{\mathbf{F1}}^{\mathtt{ref}}\mathbf{Q}_1^{\mathtt{ref}(1)} = \mathbf{F}_{\mathtt{exc}} \tag{37a}$$

$$\boldsymbol{\Phi}_{\mathbf{F2}}^{\mathtt{inc}}\mathbf{Q}_2^{\mathtt{inc}(N+1)} + \boldsymbol{\Phi}_{\mathbf{F2}}^{\mathtt{ref}}\mathbf{Q}_2^{\mathtt{ref}(N+1)} = \mathbf{0} \tag{37b}$$

The boundary condition at the left extremity of Waveguide 1 is a Dirichlet boundary condition(Equation (37a)), whereas the boundary condition at the right extremity of Waveguide 2 is a Neumann one(Equation (37b)). The continuity conditions of displacement and force between the waveguides and the coupling element form the coupling condition and can be expressed as:

$$\begin{bmatrix} \mathbf{q}_{\mathtt{LC}} \\ \mathbf{F}_{\mathtt{LC}} \end{bmatrix} = \begin{bmatrix} \mathbf{q}_{\mathtt{R1}}^{(N+1)} \\ -\mathbf{F}_{\mathtt{R1}}^{(N+1)} \end{bmatrix} \tag{38a}$$

$$\begin{bmatrix} \mathbf{q}_{\mathtt{RC}} \\ \mathbf{F}_{\mathtt{RC}} \end{bmatrix} = \begin{bmatrix} \mathbf{q}_{\mathtt{L2}}^{(1)} \\ -\mathbf{F}_{\mathtt{L2}}^{(1)} \end{bmatrix} \tag{38b}$$

where $\mathbf{q}_{\mathtt{LC}}$ and $\mathbf{F}_{\mathtt{LC}}$ stand for the nodal displacement and the nodal force at the left boundary of the coupling element, and $\mathbf{q}_{\mathtt{RC}}$ and $\mathbf{F}_{\mathtt{RC}}$ at the right boundary of the coupling element.

By substituing these continuity conditions into the dynamics of the coupling element(see Equation (17)), the boundary conditions at the right extremity of Waveguide 1 and those at the left extremity of Waveguide 2 can be obtained, as shown in Equation (39). $\mathbb{D}^*$ denotes the dynamic stiffness matrix of the coupling element condensed on the DOFs located on the interfaces between the waveguides and the coupling element itself.

$$\mathbb{D}^* \begin{bmatrix} \mathbf{q}_{\mathtt{R1}}^{(N+1)} \\ \mathbf{q}_{\mathtt{L2}}^{(1)} \end{bmatrix} = - \begin{bmatrix} \mathbf{F}_{\mathtt{R1}}^{(N+1)} \\ \mathbf{F}_{\mathtt{L2}}^{(1)} \end{bmatrix} \tag{39}$$

Combined with the boundary conditions in Equation (37a) and Equation (37b) and the propagation relation(see Equation (23)), an equation system which gives the

wave amplitudes $\mathbf{Q}$ in both waveguides under the excitation force $\mathbf{F}_{\mathbf{exc}}$ can be developed as follows:

$$\mathbf{A} \begin{bmatrix} \mathbf{Q}_1^{inc(1)} \\ \mathbf{Q}_1^{ref(1)} \\ \mathbf{Q}_2^{inc(1)} \\ \mathbf{Q}_2^{ref(1)} \end{bmatrix} = \begin{bmatrix} \mathbf{F}_{exc} \\ \mathbf{0} \\ \mathbf{0} \\ \mathbf{0} \end{bmatrix} \tag{40}$$

$$\mathbf{A} = \begin{bmatrix} \boldsymbol{\Phi}_{F1}^{inc} & \boldsymbol{\Phi}_{F1}^{ref} & \mathbf{0} & \mathbf{0} \\ (\mathbb{D}_{11}^{*}\boldsymbol{\Phi}_{q1}^{inc} + \boldsymbol{\Phi}_{F1}^{inc})\boldsymbol{\Lambda}^{N} & (\mathbb{D}_{11}^{*}\boldsymbol{\Phi}_{q1}^{ref} + \boldsymbol{\Phi}_{F1}^{ref})\boldsymbol{\Lambda}^{-N} & \mathbb{D}_{12}^{*}\boldsymbol{\Phi}_{q2}^{inc} & \mathbb{D}_{12}^{*}\boldsymbol{\Phi}_{q2}^{ref} \\ \mathbb{D}_{21}^{*}\boldsymbol{\Phi}_{q1}^{inc}\boldsymbol{\Lambda}^{N} & \mathbb{D}_{21}^{*}\boldsymbol{\Phi}_{q1}^{ref}\boldsymbol{\Lambda}^{-N} & \mathbb{D}_{22}^{*}\boldsymbol{\Phi}_{q2}^{inc} + \boldsymbol{\Phi}_{F2}^{inc} & \mathbb{D}_{22}^{*}\boldsymbol{\Phi}_{q2}^{ref} + \boldsymbol{\Phi}_{F2}^{ref} \\ \mathbf{0} & \mathbf{0} & \boldsymbol{\Phi}_{F2}^{inc}\boldsymbol{\Lambda}^{-N} & \boldsymbol{\Phi}_{F2}^{ref}\boldsymbol{\Lambda}^{N} \end{bmatrix}$$

The resolution of this equation system provides the wave amplitudes at the left boundary of the waveguides 1 and 2, and via Equation (23), wave amplitudes at any node in the two waveguides can be obtained. The nodal displacement in Z-axis at the center of the free extremity of the beam is used for the calculation of the frequency response function(FRF) of the beam. As an example, the length of the beam is chosen to be 1 m, thus $N = 97$. The pair of piezoelectric patches share the same shunt circuit with $R = 100 \; \Omega$ and $L = 2.8251 \; H$, in order to tune a flexural mode around 1350 Hz. The FRF with shunt circuit and without shunt circuit (open circuit case) are calculated numerically. Additionally, a classical finite element harmonic analysis has been performed using ANSYS to extract the FRF of the same structure in the open circuit condition. SOLID45 elements are used for the beam, and SOLID5 elements with electric potential DOF are applied for the piezoelectric patches. The finite element mesh resolutions are the same as those mentioned in subsection 3.2.1. The comparison results are displayed in Figure 14.

Figure 14

As shown in Figure 14(a), the FWFE results correspond very well to the finite element results in the frequency band from 0 to 5 kHz. The attenuation effect of the shunted piezoelectric patches around the tuning frequency (1350 Hz), which is close to the eigenfrequency of one of the flexural modes, is rather evident, as shown in Figure 14(b). In the same manner, another analysis is performed for the beam with a pair of shunted piezoelectric patches in case C displayed in Figure 13(b). The comparison results of the FRF is shown in Figure 15.

Figure 15

These results reveal again that FWFE can predict correctly the frequency response of the structure. It is an effective approach that can be employed to estimate the influence of the shunted piezoelectric patches on the flexural modes of the beam. It can be concluded from Figure 14(b) and Figure 15(b) that the longitudinally placed pair of piezoelectric patches lead to a larger attenuation frequency band than the transversally placed patches. It should also be noted that the FWFE formulation requires much less computational time compared to ANSYS. Furthermore, ANSYS is not capable of analyzing shunt circuits with negative capacitance, but the FWFE method is able to deal with all kinds of shunt impedance.

3.3 Time response calculation and reflection coefficient verification

In Subsection 3.2, the frequency responses are calculated with an excitation force of constant amplitude in the frequency domain. In order to evaluate the time response, the approach mentioned in Subsection 2.4 is carried out. The reflection coefficients can be extracted from the time response and then be compared to those calculated with the DMM approach. This extraction technique can equally be applied in experiments to validate numerical results. Let's consider an aluminium beam with a pair of longitudinally placed $R - L$ shunted piezoelectric patches. According to the dispersion curves shown in Figure 10, it can be noted that in the frequency band from 0 to 20 kHz, the bending modes are dispersive as their dispersion curves are not linear, whereas the tension/compression mode is non-dispersive as its dispersion curve is linear. As non-dispersive waves can maintain their wave form during the propagation, and their group velocity is almost constant, it will be much easier to track them in the structure. The group velocity of the tension/compression mode is shown in Figure 16. It is almost constant in the frequency band from 0 to 20 kHz. As the wavenumber of the X-axis tension/compression mode is smaller than the Z-axis bending mode, the wavelength of the former

mode is larger than the latter mode. So the same mesh resolution can be applied for the finite element models.

Figure 16

Based on this group velocity, the length of the beam is chosen to be 3 meters which is large enough so that incident and reflected waves can be clearly distinguished. To minimize the effect of induced dispersion by the piezoelectric patches, narrow band signals are used, composed of 2.5 cycles modulated by a Hanning window with the central frequency f_0 equal to 9 kHz. The time wave form and the spectrum of this wave packet excitation force is displayed in Figure 17. The maximum amplitude is 100 N and the sampling frequency is 20 times greater than the central frequency in order to guarantee the signal quality of the wave packet.

Figure 17

This excitation force is applied to one extremity of the beam as the input, and the displacement of the measure point is taken as the output, as shown in Figure 18. The measure point lies at 25 cm from the extremity with excitation force.

Figure 18

Subsequently, the forced response of the structure under white noise excitation is calculated, as shown in Figure 19. As an example, the mode at 9350 Hz is targeted,

and then the shunt circuit is tuned to this frequency, with $R = 100\ \Omega$ and $L = 0.0575\ H$.

Figure 19

From Figure 19(b), it can be seen that with the shunted piezoelectric patches, only a damping effect is obtained for the tension/compression mode, but for the flexural mode, a stronger attenuation effect is achieved, as shown in Figure 14(b), where the shunted piezoelectric patches play the role of a dynamic damper which creates an added DOF in the system. With the transfer function, the wave packet excitation is applied to the system in order to acquire the frequency response. Then the IDFT of this frequency response is carried out to calculate the time response of the structure, as displayed in Figure 20. As those wave packets are apparently unconnected in this case, no wave packet decomposition techniques are needed.

Figure 20

It can be noted that when the beam is equipped with the piezoelectric patches, the reflection of the tension/compression wave is no longer null due to the added mass and stiffness. When the shunt circuit is applied onto the piezoelectric patches, the reflection becomes stronger and the damping effect can be observed in the reflected packet. In order to verify the reflection coefficients calculated via the DMM approach and provide an effective experi-

mental evaluation technique for the reflection coefficient based on time response of the structure, the following extraction procedure is proposed:

1. The Hilbert Transform is applied to the time response of the structure, and its absolute value is representative of the envelope of the signal. The first peak represents the maximum amplitude of the incident wave, and the second peak for the reflected wave, as shown in Figure 21.

Figure 21

2. The imaginary part of the wavenumber k calculated with the WFE method is used to calculate the spatial damping. As the propagation of this mode can be characterized by an exponential law $A = A_0 e^{ikx}$, the spatial damping ratio $\gamma_x = -\mid Im(k) \mid$.

3. With the group velocity V_g of this wave mode, the damping ratio in time domain can be calculated as $\gamma_t = -\mid Im(k)V_g \mid$.

4. On the plot of the Hilbert Transform result, a damping curve can be drawn to take into account the damping effect caused by the distance between the measure point and the piezoelectric patches so as to evaluate the reflection coefficient correctly. This curve passes the first peak of the Hilbert Transform result and follows the exponential decreasing law defined by $A = A_0 e^{\gamma_t t}$. $\mathbf{A_r}$ denotes the amplitude

of the reflected wave, and $\mathbf{A_i}$ represents the amplitude of the incident wave with the attenuation effect taken into account, as shown in Figure 21. The reflection coefficient can be calculated as $\mathbf{R = A_r/A_i}$.

5. By varying the central frequency f_0 of the wave packet excitation, reflection coefficients at different frequencies can be acquired frequency by frequency in order to verify the reflection coefficients calculated with the DMM approach.

The reflection coefficients of the tension/compression mode tuned at 9350 Hz are calculated via the DMM approach, and then compared to those obtained through the extraction procedure. It should be mentioned that this extraction procedure is a rather coarse evaluation tool for the reflection coefficients. If an error of $\pm 10\%$ is applied to each extracted reflection coefficient, then the envelope of the extracted reflection coefficients can be obtained. The results are shown in Figure 22.

Figure 22

For the frequency band below 7 kHz, it is difficult to evaluate correctly the reflection coefficient with the extraction procedure as the span of the wave packet in time domain becomes so large that it's hard to distinguish incident and reflected waves, unless the length of the beam becomes larger. And for the frequency band around the tuning frequency, it is also difficult

to evaluate precisely the reflection coefficient with the Hilbert Transform, as the added damping effect needs to be considered properly. But globally, the results issued from the DMM approach are verified by those through the extraction procedure, as the envelope covers most of the DMM results in the open circuit case. This procedure will be employed for the experimental validation of numerically calculated reflection coefficients.

4 Conclusions

Effective prediction tools for wave propagation characteristics and dynamic behavior of smart structures equipped with shunted piezoelectric elements are provided in this work, and general formulations which can be applied for all kinds of slender smart structures are developed. The main results can be summarized as follows:

– The finite element based WFE approach is developed and its corresponding DMM model is extended to consider shunted piezoelectric elements in beam structures. The wave modes propagating in the structure are correctly captured and the influence of the shunted piezoelectric patches on the control of the Z-axis flexural wave mode is investigated through

the reflection and transmission coefficients of this wave mode.

– An analytical model based on Euler-Bernoulli beam theory, the homogenization of sandwich beams and Hagood's shunted piezoelectric patch model is developed to verify numerically calculated reflection and transmission coefficients of the Z-axis flexural mode.

– The forced responses of the beam structure excited in the Z-axis flexural mode and the X-axis tension/compression mode are calculated via the FWFE formulation, and the results for the Z-axis flexural mode correspond very well with those issued from a classical FE harmonic analysis.

– Time response of the structure excited in the X-axis tension/compression mode with wave packet is evaluated via an IDFT approach applied to the frequency response. By following an extraction procedure, reflection coefficients of this wave mode can be evaluated according to the time response of the structure so as to verify the reflection coefficients calculated through the DMM approach.

The numerical techniques presented in this work enable the evaluation of the performance of shunted piezoelectric patches on the control of flexural wave propagation, and facilitate design modifications and systematic investigations of geometric and electric parameters of beam structures with shunted piezoelectric patches. Future work aims at the experimental validation of the numerical results. Numerical investigation of structures with multiple shunted piezoelectric patches and corresponding experimental validations will be carried out as well.

Appendix A: material properties of the piezoelectric patch (type SG P189)

Mass density ρ: $\rho = 7650 \ kg/m^3$.

Material stiffness matrix $\mathbf{c}^E$:

$$\mathbf{c}^E = 10^{10} \times \begin{bmatrix} 15.37 & 8.23 & 8.06 & 0 & 0 & 0 \\ 8.23 & 15.37 & 8.06 & 0 & 0 & 0 \\ 8.06 & 8.06 & 13.74 & 0 & 0 & 0 \\ 0 & 0 & 0 & 4.59 & 0 & 0 \\ 0 & 0 & 0 & 0 & 4.59 & 0 \\ 0 & 0 & 0 & 0 & 0 & 3.57 \end{bmatrix} \ Pa$$

The piezoelectric stress coupling matrix $\mathbf{e}$:

$$\mathbf{e} = \begin{bmatrix} 0 & 0 & 0 & 0 & 12.88 & 0 \\ 0 & 0 & 0 & 12.88 & 0 & 0 \\ -6.187 & -6.187 & 12.80 & 0 & 0 & 0 \end{bmatrix} \ N/(V \cdot m)$$

The permittivity matrix under constant strain ϵ^S:

$$\epsilon^S = 10^{-8} \times \begin{bmatrix} 1.011 & 0 & 0 \\ 0 & 1.011 & 0 \\ 0 & 0 & 0.591 \end{bmatrix} C/(V \cdot m)$$

References

1. M. Collet, V. Walter, P. Delobelle, Journal of Sound and Vibration **260**(3), 453 (2003)

2. Y. Meyer, T. Verdot, M. Collet, Journal of Smart Materials and Structures **16**(1), 128 (2007)

3. M. Collet, K.A. Cunefare, M.N. Ichchou, Journal of Intelligent Material Systems and Structures **20**(7), 787 (2009)

4. N.W. Hagood, A. Flotow, Journal of Sound and Vibration **146**, 243 (1991)

5. O. Thorp, M. Ruzzene, A. Baz, Journal of Smart Materials and Structures **10**(5), 979 (2001)

6. A. Spadoni, M. Ruzzene, K.A. Cunefare, Journal of Intelligent Material Systems and Structures **20**(8), 979 (2009)

7. C.H. Nguyen, S.J. Pietrzko, Finite elements in analysis and design **42**(14-15), 1231 (2006)

8. J. Becker, O. Fein, M. Maess, L. Gaul, Computers and Structures **84**(31-32), 2340 (2006)

9. F. Casadei, M. Ruzzene, L. Dozio, K.A. Cunefare, Journal of Smart Materials and Structures **19**(1) (2010). 015002

10. E. Crawley, J. de Luis, AIAA Journal **25**, 1373 (1987)

11. C.K. Lee, The Journal of the Acoustical Society of America **87**(3), 1144 (1990)

12. X.D. Zhang, C.T. Sun, Smart Materials and Structures **5**(6), 814 (1996)

13. Y.H. Hu, W.Y. Yao, Smart Materials and Structures **16**(3), 706 (2007)

14. C. Park, Journal of Sound and Vibration **268**(1), 115 (2003)

15. A. Benjeddou, Computers and Structures **76**, 347 (2000)

16. W.X. Zhong, F. Williams, Journal of Sound and Vibration **181**(3), 485 (1995)

17. J.M. Mencik, M.N. Ichchou, European Journal of Mechanics - A/Solids **24**(5), 877 (2005)

18. J.M. Mencik, M.N. Ichchou, International Journal of Solids and Structures **44**, 2148 (2007)

19. M.N. Ichchou, S. Akrout, J.M. Mencik, Journal of Sound and Vibration **305**, 931 (2007)

20. B.R. Mace, D. Duhamel, M.J. Brennan, L. Hinke, Journal of Acoustical Society of America **117**(5), 2835 (2005)

21. D. Duhamel, B.R. Mace, M.J. Brennan, Journal of Sound and Vibration **294**(1-2), 205 (2006)

22. B.R. Mace, E. Manconi, Journal of Sound and Vibration **318**(4-5), 884 (2008)

23. M. Collet, M. Ouisse, M. Ruzzene, M.N. Ichchou, International Journal of Solids and Structures **48**(20), 2837 (2011)

24. A. Chen, F. Li, Y. Wang, Journal of Sound and Vibration **304**(3-5), 863 (2011)

25. M. Leamy, Journal of Sound and Vibration **331**(7), 1580 (2012)

26. G. Wang, S. Chen, J. Wen, Smart Materials and Structures **20**(1), 015026 (2011)

27. M.N. Ichchou, J.M. Mencik, W. Zhou, Computer methods in applied mechanics and engineering **198**(15-16), 1311 (2009)

28. T.L. Huang, M.N. Ichchou, O.A. Bareille, Structural Control and Health Monitoring (DOI: 10.1002/stc.451) (2011)

29. Y. Waki, B.R. Mace, M. Brennan, Journal of Sound and Vibration **327**, 92 (2009)

30. J. Renno, B. Mace, Journal of Sound and Vibration **329**, 5474 (2010)

31. Y. Yong, Y.K. Lin, Journal of Sound and Vibration **129**(2), 99 (1989)

32. J.M. Mencik, M.N. Ichchou, L. Jézéquel, Revue Européenne de Mécanique Numérique **15**(1-3), 293 (2006)

33. B.R. Mace, Journal of Sound and Vibration **97**, 237 (1984)

34. J. Murin, M. Aminbaghai, V. Kutis, Engineering structures **32**(6), 1631 (2010)

35. N.G. Stephen, Journal of Sound and Vibration **227**, 1133 (1999)

36. G. Dai, W. Zhang, Acta Mechanica Sinica **25**(6), 353 (2009)
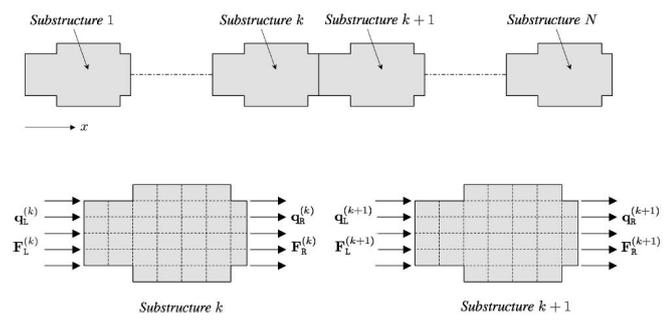
Fig. 1 An illustration of a periodic waveguide [17].
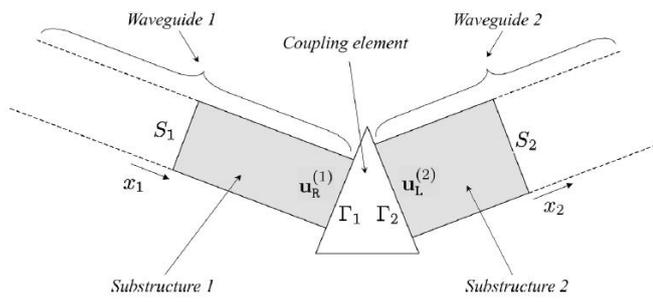
Fig. 2 An illustration of the coupling between two different periodic waveguides [17].
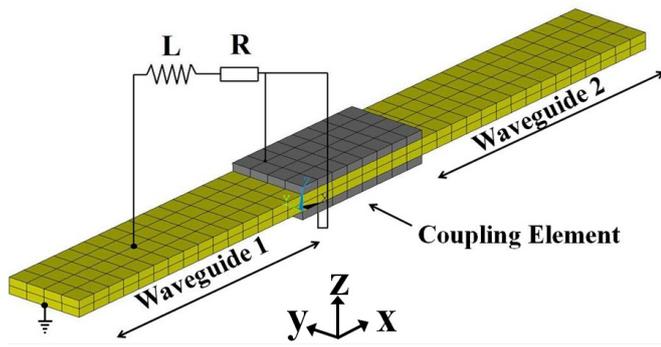
Fig. 3 Finite element model of a beam with symmetric shunted piezoelectric patches. The coupling element is the part of the beam with the two symmetric piezoelectric patches.
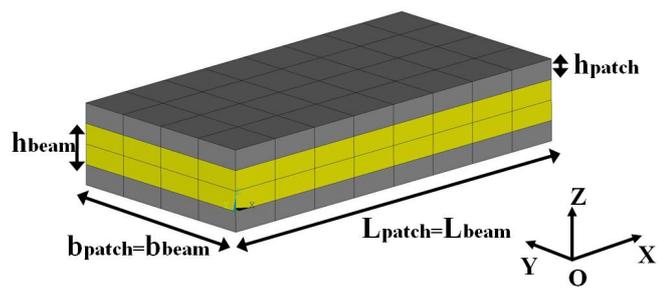
Fig. 4 Finite element model of the coupling element and definition of geometric parameters in case A.
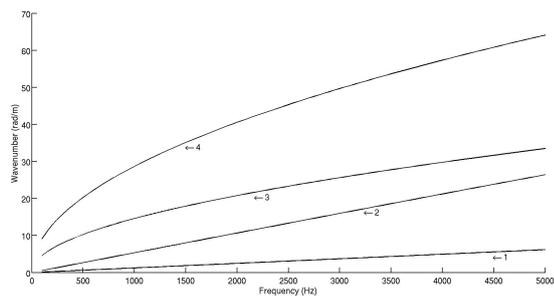
Fig. 5 Dispersion curves of the wave modes propagating in the beam in case A: (1)Tension/compression wave in X-axis (2)Torsional wave in X-axis (3)Flexural wave in Y-axis (4)Flexural wave in Z-axis. These wave modes are identified through their mode shapes (eigenvectors) issued from the WFE approach.
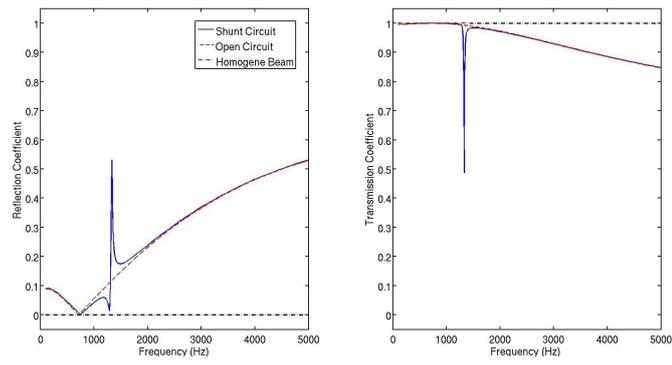
**Fig. 6** Reflection and transmission coefficients of the Z-axis flexural wave mode propagating in the beam in case A. (Solid line)With R-L shunt circuit (Dashed line)Open circuit (Dash-dotted line)Beam without piezopatches.
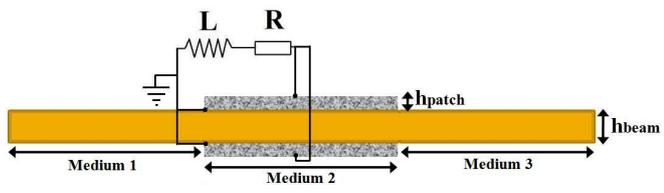
Fig. 7 Homogenized Euler-Bernoulli beam model with two

symmetric R-L shunted piezoelectric patches.
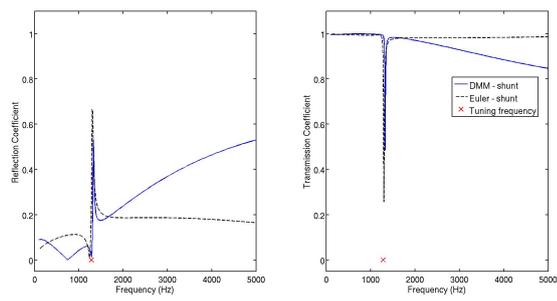
Fig. 8 Comparison of reflection and transmission coefficients of the flexural mode in Z-axis between the results of the homogenized Euler-Bernoulli beam model and those of the DMM approach in case A. (Solid line)DMM results (Dashed line)Homogenized model results.
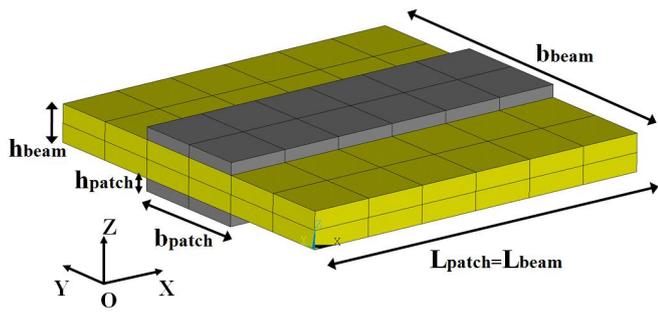
(a)
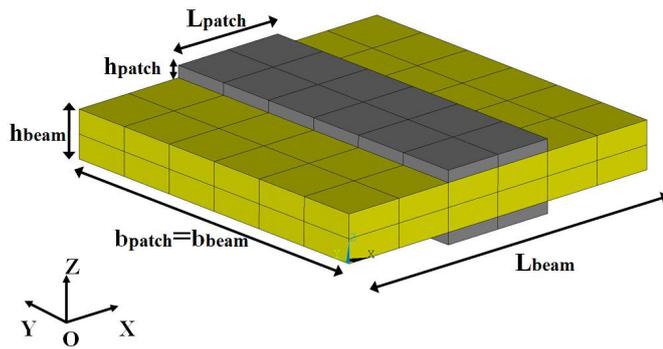
(b)

Fig. 9 Finite element model of the coupling element and definition of geometric parameters (a)in case B: the two piezoelectric patches are placed longitudinally (b)in case C: the two piezoelectric patches are placed transversally.
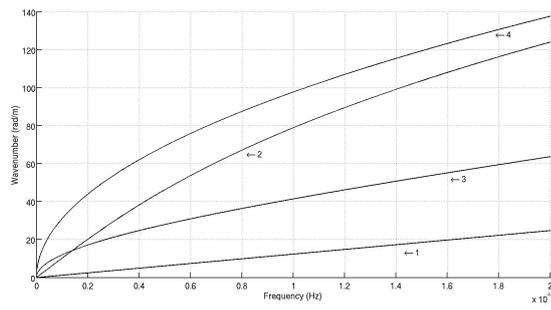
Fig. 10 Dispersion curves of the wave modes propagating in the beam in case B and case C: (1)Tension/compression mode in X-axis (2)Torsional wave in X-axis (3)Flexural wave in Y-axis (4)Flexural wave in Z-axis. These wave modes are identified through their mode shapes (eigenvectors) issued from the WFE approach.
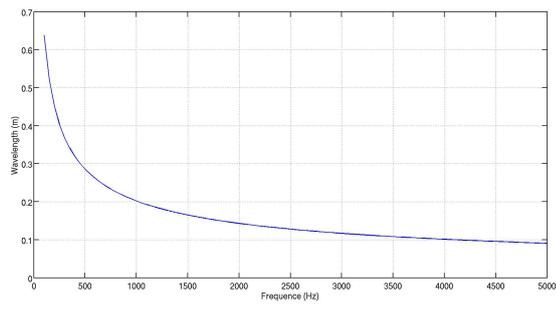
Fig. 11 Wavelength of the flexural wave in Z-axis in case B

and case C.
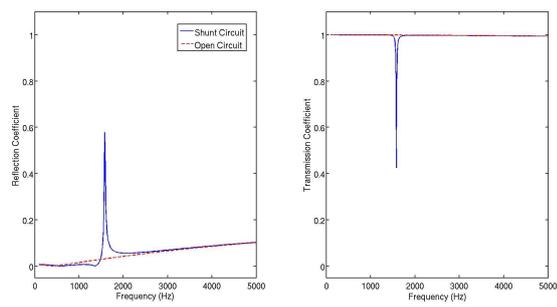
(a)
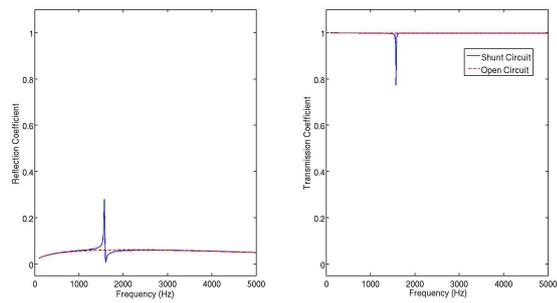
(b)

Fig. 12 Reflection and transmission coefficients of the Z-axis flexural wave mode propagating in the beam (a)Case B (b)Case C. (Solid line)With R-L shunt circuit. (Dashed line)Open circuit.
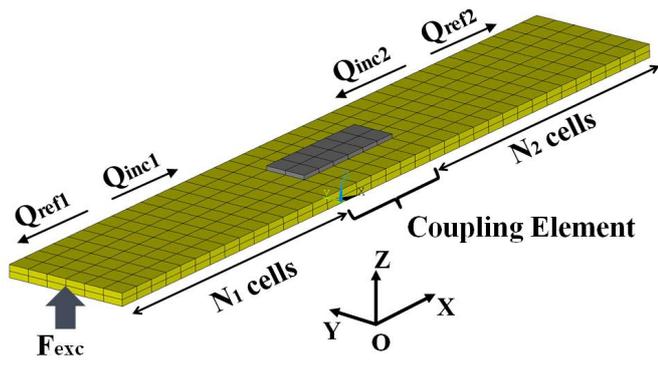
(a)
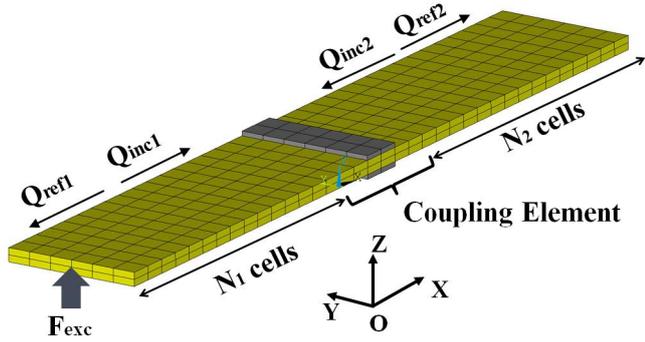
(b)

Fig. 13 WFE model for the calculation of the forced response of the beam with shunted piezoelectric patches (a)in case B (b)in case C
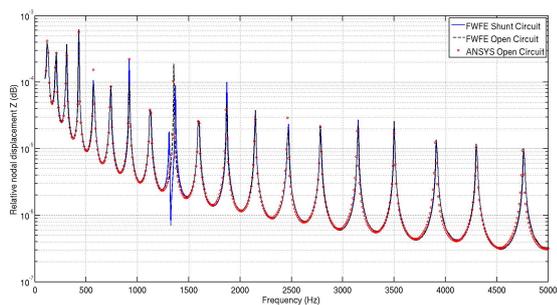
(a)
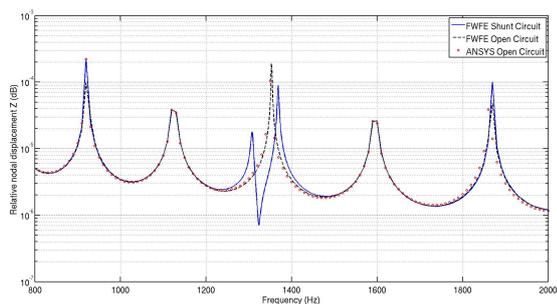
(b)

Fig. 14 Comparison of the frequency responses in case B: (a)Frequency band from 0 to 5 kHz (b)Zoom around the tuning frequency (1350 Hz).(Solid line)FWFE with shunted circuit. (Dashed line)FWFE without shunt circuit. (∘ markers)ANSYS results without shunt circuit.
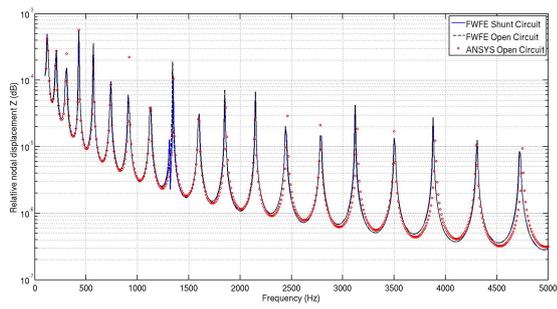
(a)
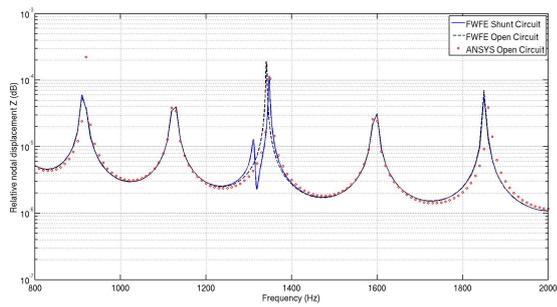
(b)

Fig. 15 Comparison of the frequency responses in case C: (a)Frequency band from 0 to 5 kHz (b)Zoom around the tuning frequency (1350 Hz). (Solid line)Piezoelectric patches with shunted circuit. (Dashed line)Piezoelectric patches without shunt circuit. (○ markers)ANSYS results without shunt circuit.
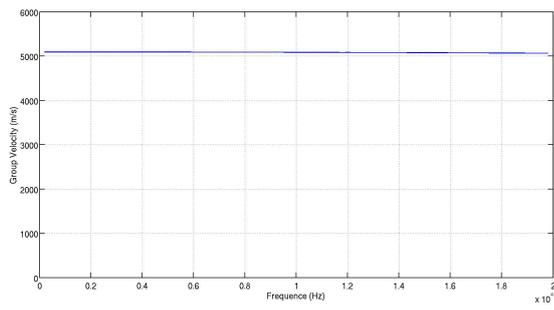
Fig. 16 Group Velocity of the tension/compression wave in

X-axis in case B.
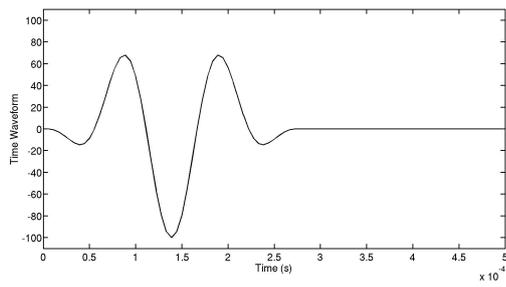
(a)
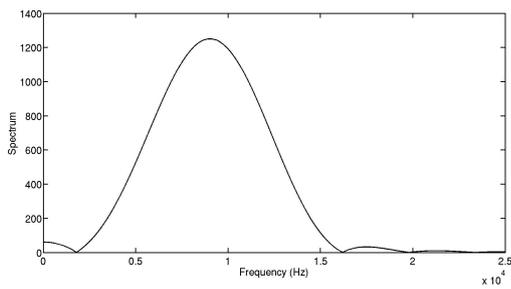
(b)

Fig. 17 The time wave form and the spectrum of the wave

packet excitation. (a)Time wave form (b)Spectrum.
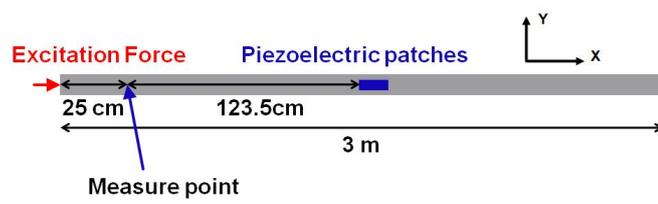
Fig. 18 Configuration for the time response simulation of the tension/compression wave in X-axis.
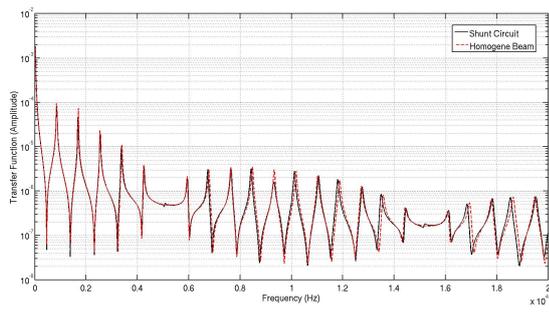
(a)
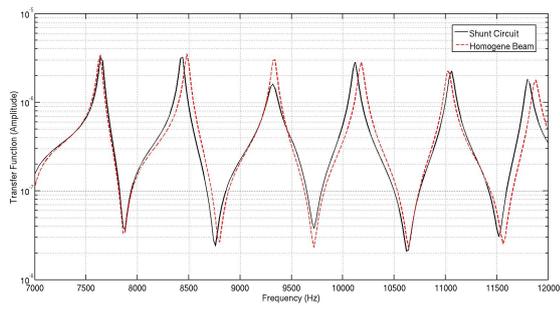
(b)

Fig. 19 The forced response of the structure under white noise excitation (transfer function) tuned at 9350 Hz. (a)Frequency response (b)Zoom around the tuning frequency. (Solid line)Piezoelectric patches with shunted circuit. (Dashed line)Beam without piezoelectric patches.
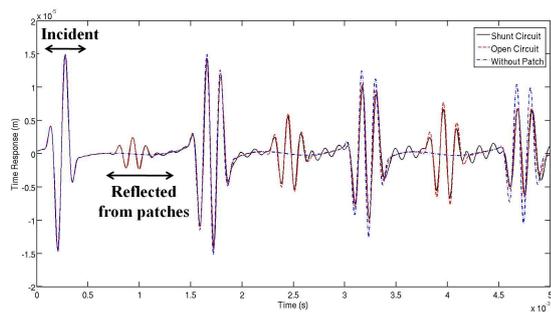
Fig. 20 Time response of the structure under wave packet excitation. (Solid line)Piezoelectric patch with shunt circuit. (Dashed line)Piezoelectric patches without shunt circuit. (Dash-dotted line)Beam without piezoelectric patches.
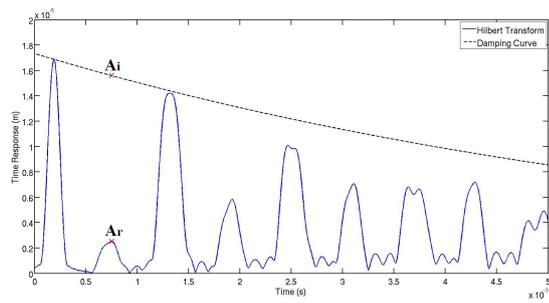
Fig. 21 Hilbert Transform of the time response and the damping curve to extract the reflection coefficient of the tension/compression wave. (Solid line)Absolute value of the Hilbert Transform of the time response. (Dashed line)Damping curve based on spatial damping.
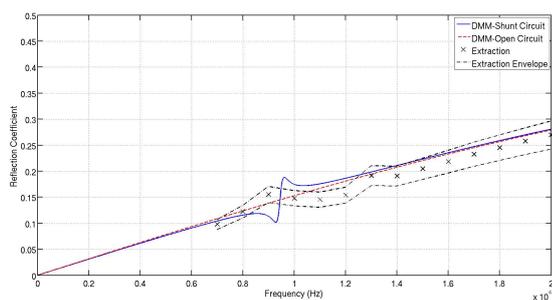
Fig. 22 Comparison of reflection coefficients of the tension/compression wave in X-axis calculated through the DMM approach and the extraction procedure. (Solid line)Calculation with DMM, piezoelectric patch with shunt circuit. (Dashed line)Calculation with DMM, piezoelectric patch without shunt circuit. ($\times$ markers)Calculation with extraction procedure. (Dash-dotted line)Envelope of the extracted reflection coefficients.

Table 1 Numeric values of the geometric parameters in the coupling element shown in Figure 4(case A), Figure 9(a)(case B) and Figure 9(b)(case C). The units of all the parameters are in meter (m).

Case	L_{beam}	L_{patch}	b_{beam}	b_{patch}	h_{beam}	h_{patch}
A	0.04	0.04	0.02	0.02	0.004	0.002
B	0.03	0.03	0.03	0.01	0.003	0.001
C	0.03	0.01	0.03	0.03	0.003	0.001